Atmos. Meas. Tech. Discuss., 8, 9241–9287, 2015
www.atmos-meas-tech-discuss.net/8/9241/2015/
doi:10.5194/amtd-8-9241-2015

Atmospheric Measurement Techniques Discussions

Multi-sensor analysis of convective activity in Central Italy during the HyMeX SOP 1.1

N. Roberto[1], E. Adirosi[1], L. Baldini[1], D. Casella[1], S. Dietrich[1], P. Gatlin[2], G. Panegrossi[1], M. Petracca[1,3], P. Sanò[1], and A. Tokay[4,5]

[1]CNR – Istituto di Scienze dell'Atmosfera e del Clima, Roma, Italy
[2]NASA Marshall Space Flight Center, Huntsville, Alabama
[3]Department of Physics, University of Ferrara, Ferrara, Italy
[4]Joint Center for Earth Systems Technology, University of Maryland Baltimore County, Baltimore, MD, USA
[5]NASA Goddard Space Flight Center, Greenbelt, MB, USA

Received: 30 July 2015 – Accepted: 2 August 2015 – Published: 7 September 2015

Correspondence to: N. Roberto (nicoletta.roberto@artov.isac.cnr.it)

Published by Copernicus Publications on behalf of the European Geosciences Union.

Abstract

A multi-sensor analysis of convective precipitation events that occurred in central Italy, in autumn 2012 during the HyMeX (Hydrological cycle in the Mediterranean eXperiment) Special Observation Period (SOP) 1.1 is presented. Various microphysical properties of liquid and solid hydrometeors were examined to assess their relationship with lightning activity. The instrumentation used consisted of a C-band dual-polarization weather radar, a 2-D video disdrometer, and a lightning network. A fuzzy logic based hydrometeor classification algorithm was tuned and optimized for the detection of graupel from C-band dual-polarization radar measurements. Graupel ice water content was then retrieved and related to lightning activity. A linear correlation was found between the total mass of graupel above the 0° isothermal and the number of strokes detected by the lightning network in agreement with model outputs, which confirms the importance of ice in the electrical charging of convective clouds, although differences were noticed among events. Parameters of the gamma raindrop size distribution measured by a 2-D video disdrometer, revealed the transition from convective to stratiform regime during the event and where related. However, lightning activity was not always recorded when the precipitation regime was classified as convective. More robust relationships were found relating lightning activity to graupel.

1 Introduction

Cloud microphysical processes and their relation to the electrical activity during intense convective precipitation events is an issue of strong interest, especially for its impact on Numerical Weather Prediction (NWP) models. The contribution of very fine-scale kinematic and microphysical processes and their non-linear interactions with larger scale processes limit the ability of current NWP models to predict these phenomena (e.g., Weisman et al., 2008; Miglietta and Rotunno, 2012). Many projects and fields campaigns aimed at investigating convection by deploying ground and airborne instruments

AMTD
8, 9241–9287, 2015

have been conducted but especially in the US and in tropical regions, most recent one being the multi-year and multi-site Chuva in Brazil (Machado et al., 2013), or the Mid-latitude Continental Convective Clouds Experiment (MC3E) in Oklahoma (Petersen and Jensen, 2012). Although similar experiments are not so frequent in Mediterranean, the ongoing Hydrological cycle in the Mediterranean eXperiment (HyMeX) includes some experimental activity to investigate convection. In particular, the special observation period (SOP) 1.1 that took place between 5 September and 6 November 2012 in target regions of the Mediterranean basin was dedicated to observing heavy precipitation and flash-floods (Ducrocq et al., 2014). Several instrumented hydro-meteorological sites were set-up and three of them were in Italian regions – Liguria-Tuscany (LT), North-Eastern Italy (NEI), and Central Italy (CI) – where mechanisms responsible for most of the heavy precipitation and flood events in the northwestern Mediterranean have been found to exist (see Ferretti et al., 2014; for an overview of activities in Italy). The CI site is of particular interest both for its central position between the Adriatic Sea and the Tyrrhenian Sea, and because it includes the densely populated urban area of Rome that consists of approximately 4 million inhabitants. In the late summer-early autumn, severe weather conditions in CI are quite frequent and are mostly related to the development of intense convective systems (Melani et al., 2013). The correct forecast of precipitation associated with these events is linked to the ability of numerical models to initiate convection, which is especially challenging over the Tyrrhenian Sea, and with the correct representation of cloud microphysical processes (Ferretti et al., 2014). The microphysical schemes used by NWP models often misrepresent the auto-conversion processes as well as the characteristics of cloud particles (e.g., size distribution, densities, etc.). The microphysical parameterization should be tuned to the different types of precipitation regimes (i.e., convective vs. stratiform) throughout the lifecycle of the simulated event (Lang et al., 2003; Wu et al., 2013). Ground-based instruments such as weather radars and disdrometers can be used to gain insight about the microphysical structure of a precipitating cloud and to derive the parameters required by microphysics schemes. Lightning information is useful to monitor the evolution of convective events

AMTD
8, 9241–9287, 2015

(e.g., Gatlin and Goodman, 2010) as well as to assess the NWP model ability to reproduce their intensity and predict their evolution in time (e.g., Federico et al., 2014). Robust relationships between cloud microphysics (and dynamics, i.e. updraft strength) and lightning activity could be exploited during assimilation of lightning data into NWP models to improve the initiation and forecast in both time and space of convective activity (Lynn et al., 2012; Lagouvardos et al., 2013).

Numerous studies have investigated the relationship between lightning and heavy precipitation, and, more specifically, the relationship between the volume of precipitable water and lightning flashes that was found variable on the climatology as well as geographical location (e.g., Petersen and Rutledge, 1998 and references therein; Lang and Rutledge, 2002; Latham et al., 2003; Albrecht et al., 2011). However, the relationship between total lightning activity and ice mass appears to be more robust (Petersen et al., 2005; Deierling et al., 2008; Formenton et al., 2013). The non-inductive mechanism of charging clouds considered to be the principal source of charge involved in lightning flashes within thunderstorms (Saunders, 1993; Latham et al., 2007) is mainly related to the collisions between cloud ice crystals (charged positively) and graupel (charged negatively), suggesting a relation between ice mass and the amount of lightning activity. Several studies over the last decade have shown that dual-polarization radar measurements may exhibit signatures that can be tied to lightning flash rate (e.g., Lopez et al.,1997; Goodman et al., 1989; Carey and Rutledge,1996; Wiens et al., 2005). Lopez and Aubagnac (1997) showed that the evolution of lightning activity in an Oklahoma supercell thunderstorm that produced copious amounts of hail was related to changes in the microphysical characteristics of the storm inferred from polarimetric radar. Their results indicate that the development of graupel above the freezing level is related to the overall increase/decrease in the number of cloud to ground (CG) flashes. Contributions concerning quantitative relationships between graupel mass and lightning activity come from studies based on satellite observations or numerical cloud electrification models, rather than on ground based weather radar. Petersen et al. (2005) used cloud ice microphysical information obtained from the Precipitation Radar (PR)

AMTD
8, 9241–9287, 2015

onboard the National Aeronautics and Space Administration (NASA) Tropical Rainfall Measuring Mission (TRMM) satellite to find global relationships between ice water content and lightning activity observed by the Lightning Imaging Sensor (LIS) onboard TRMM. They found that, on a global scale, the relationship between columnar precipitation ice mass and lightning flash density is invariant between land, ocean and coastal regimes. Formenton et al. (2013) showed a quantitative relation between columnar graupel mass content and flash rate using a one-dimensional numerical cloud electrification model.

Rain at ground, characterized by its raindrop size distribution (RSD), the number concentration of rain drops as a function of their equivolume diameter, is measured at ground by raindrop sampling instruments (disdrometers). RSD can present distinctive properties allowing to classify rain as convective or stratiform (e.g., Bringi et al., 2003; Friedrich et al., 2013) and, possibly, could be related to lightning activity.

This study attempted to: (1) show that ground-based instruments deployed in CI during the SOP 1.1 (weather radar, and disdrometers) provide useful insight into the microphysical structure and evolution of precipitating clouds, and (2) examine the relationship between the microphysical parameters estimated by the different instruments and the cloud electrical activity. Investigation is based on a subset of instruments of the CI hydro-meteorological site, namely a ground-based lightning sensor network, a scanning C-band dual polarization radar, which was installed in the southeastern part of Rome, and a nearby instrumented site (14 km from the C-band radar, in the historic center of Rome) that included a disdrometer. In such configuration, dual-polarization radar is used to estimate the ice mass content, while RSD are estimated from disdrometer observations. Both estimates are analyzed in relation to the number of total lightning strokes detected by the ground-based lightning detection network.

Section 2 presents the instrumentation used and some issues related to data quality. In Sect. 3 the techniques employed to retrieve graupel properties and RSD as well as process lightning data are described. The dataset and details of selected case studies

AMTD
8, 9241–9287, 2015

are given in Sect. 4, while Sect. 5 discusses important results. Our conclusions can be founded in the last section of this paper.

2 Instrumentation

Several instruments were made available during the HyMeX SOP1.1 to be deployed in the CI hydro-meteorological site (Ferretti et al., 2014) thanks to the cooperation amongst the Italian meteorological services and the scientific community, as well as contribution from NASA GPM Ground Validation Programme. Instruments selected for this study included the dual-polarization C-band radar (Polar 55C) of the Nation Research Council of Italy, Institute of Atmospheric Science and Climate (CNR-ISAC), a 2-dimensional video disdrometer (2-DVD), which is located in the historic center of Rome and the European LIghtning detection NETwork (LINET; Betz et al., 2009).

LINET provides detection of total lightning, which is composed of cloud-to-ground (CG) lightning and intra-cloud (IC) lightning, by utilizing Very Low Frequency/Low Frequency (VLF/LF) techniques (i.e., 10 frequency intervals between 1 and 200 KHz). More than 120 sensors in over 20 European countries compose the network with good coverage of the central and western Mediterranean region, from 10° W to 35° E in longitude and from 30 to 65° N in latitude. Further details and specifications are in Betz et al. (2009) and Federico et al. (2014). The detection efficiency of ICs and CGs depends on the distance between the stroke event and the LINET sensors. In the border areas of the network (e.g. the Mediterranean), baselines between stations are larger, which causes lower detection efficiency in these areas and thus weak IC and CG signals are not properly located (Zinner et al., 2013).

A 2-DVD (compact version) by Joanneum Research mbH, Graz, Austria (Schönhuber et al., 2008) was installed on the roof of the Department of Electrical Engineering and Telecommunications at Sapienza University of Rome (hereinafter “Sapienza site”, 41.89° N, 12.49° E, and 70 m a.s.l.). The 2-DVD is an optical disdrometer that provides properties of raindrops such as diameter, fall velocity and oblateness of each particle

AMTD
8, 9241–9287, 2015

(Schönhuber et al., 2008). Drop size and drop velocity measured by the 2-DVD are more accurate across a broad spectrum of drop sizes than the similar measurements collected by disdrometers employing different measuring principles (Tokay et al., 2013).

Polar 55C is a research grade C-band (5.6 GHz) dual-polarization Doppler radar located on outskirts of Rome (41.84° N, 12.65° E, and 130 m a.s.l.) 14 km south-east of the Sapienza site (Sebastianelli et al., 2013). Radar measurements were collected using a pulse duration of 0.5 µs (corresponding to range resolution of 75 m) and a pulse repetition frequency of 1200 Hertz. The scanning strategy was configured as follows: (i) a volume scan consisting of unevenly spaced elevation angles to obtain a vertical resolution of 1 km above the Sapienza site (elevation angles in degree are 0.6, 1.6, 2.6, 4.4, 6.2, 8.3, 11.0, 14.6), (ii) scans at vertical incidence, and (iii) RHIs directed toward the Sapienza site. Tasks (ii) and (iii) were added to the volume scan depending on the presence of precipitation above the Polar 55C and the Sapienza site, respectively. The scanning strategy was designed to provide an update every 5 min. During the SOP, the Polar 55C performed also operator-supervised RHI scans along the route of a research aircraft (the *Falcon* 20 of Service des avions français instrumentés pour la recherche en environnement that did not flight over CI during convection).

3 Analysis techniques

3.1 Radar graupel detection and IWC estimation

Dual polarization radar backscattering and propagation measurements are sensitive to cloud properties and vary with the size, shape, concentration, habit, and fall velocity of liquid and ice hydrometeors. For this reason, dual-polarization radar is capable of identifying the type of hydrometeors that dominate a radar resolution volume by means of Hydrometeor Classification Algorithms (HCA) that are exploited in this study to identify graupel. Several observational studies have employed dual-polarization radar to relate microphysical properties of convective cloud to the electrical activity (Lopez et al., 1997;

AMTD
8, 9241–9287, 2015

Wiens et al., 2005). While most of them used radar measurements to detect ice mass by tracking one or more convective cells during their life cycle, Polar 55C radar measurements were employed in this study to characterize the ice mass of graupel during the entire convective event within 120 km of the radar. Once radar resolution volumes containing graupel are identified, graupel ice mass is computed from reflectivity factor measurements utilizing a power law relation.

3.1.1 Radar scattering properties of graupel

The electromagnetic scattering properties of graupel were obtained using the T-matrix method (Barber and Yeh, 1975) to: (1) define proper membership functions for graupel identification by means of a fuzzy logic HCA, and (2) obtain a simple algorithm to retrieve the ice water content of graupel from measured radar reflectivity factor. A broad population of graupel particle size distributions (PSD) was obtained by randomly varying parameters of an exponential PSD in the form

$$N(D) = N_0 \exp[-3.67(D/D_0)] \quad (1)$$

where N_0 ($\mathrm{mm}^{-1}\,\mathrm{m}^{-3}$) is the intercept parameter of the size distribution, D is the equivalent volume particle diameter (in mm), and D_0 is the median volume diameter (in mm). T-matrix simulations were performed for temperatures between −15 °C and +5 °C, liquid water fractions between 5 and 55 %, and particle densities between 0.2 and 0.9 $\mathrm{g\,cm}^{-3}$ (Pruppacher and Klett, 1978; Dolan and Rutledge, 2009; Dolan et al., 2013). The microphysical parameters used for simulations are summarized in Table 1.

Graupel can take on different shapes, primarily hexagonal, lump, spheroidal and conical, which are difficult to identify using polarimetric radar. Some classification algorithms do not distinguish graupel from small and dense ice hydrometeors, such as small hail, while others categorize it as either low density or high-density graupel (Dolan et al., 2013). In addition to the spheroidal shape, the presence of conical shapes has been inferred from polarimetric radar measurements of differential reflectivity (Evaristo

AMTD
8, 9241–9287, 2015

et al., 2013). Therefore, two different simulations were performed to model graupel as having either spheroidal or conical shape by differing the axis ratio (ratio of semi-minor to semi-major axis) and canting angles. The mathematical formulation described by Wang (1982) was used for modelling conically shaped graupel. The fall behaviour of graupel, especially its orientation, is not well established, and some investigators have hypothesized that the larger rimed ice particles probably tumble, though conical graupel may have a preferential fall orientation (Pruppacher and Klett, 1978) that oscillate ±20° about its vertical axis (Zikmunda and Vali, 1972). Some graupel can fall with an axis ratio exceeding one (prolate) and other graupel with an axis ratio less than one (oblate) (Wang, 1982). For conical shapes, we randomly varied the axis ratio between 0.75 and 1.1 (Heymsfield, 1972) with a zero mean Gaussian canting angle distribution and a standard deviation varying from 0 to 30°. For spheroidal shapes, we varied the canting angle standard deviation from 0 to 15° and the axis ratio randomly between 0.9 and 1. Figure 1 shows the output of simulated dual-polarization radar observables for spheroidal (a, c), and conical (b, d) shaped graupel. Observing the four scatter plots Z_h of the graupel PSDs ranged from around 10 to 60 dBZ for both shapes. While Z_{dr} was between 0 and 1 dB for spheroidal shapes, and it covered a 1.5 dB wider range including slightly negative values and maximum value near 2 dB for conical shapes (Fig. 1a and b). The simulated K_{dp} values also exhibited larger variation for the conical shapes (Fig. 1c and d).

3.1.2 Graupel identification

The results of the electromagnetic simulations were used to define proper beta membership functions of a Fuzzy Logic (FL) hydrometeor classification algorithm (Liu and Chandrasekar, 2000; Lim and Chandrasekar, 2005) tailored for C-band and graupel detection. Inputs of the FL classificator are the Polar 55C radar measurements of Z_h, Z_{dr}, K_{dp}, the standard deviation of the differential propagation phase shift (ϕ_{dp}), which was calculated in a 375 m range moving window (i.e., five 75 m range bins), and the height of the top of the melting layer (ML). Measurements of Z_h and Z_{dr} were corrected

AMTD
8, 9241–9287, 2015

for attenuation by utilizing linear relations between specific attenuation at horizontal polarization, specific differential attenuation and K_{dp} (parameterizations are in Baldini et al., 2014) that were applied to propagation paths below the 0 °C level. The height of the top of ML is considered to be the 0 °C level from vertical temperature soundings collected at the nearby Pratica di Mare airport. For each radar measurement bin, the FL scheme assigns a score to each radar measurement. These scores are obtained by considering how the radar measurements fit the set of membership functions for a given hydrometeor type. The hydrometeor type with the highest score is assigned to each radar resolution volume. The results of the simulations of Fig. 1 have been used to tune the membership functions for graupel. The membership functions of Z_{dr} and K_{dp} were set to account for both spheroidal and conical shaped graupel by allowing Z_{dr} to vary between −1 and 2 dB and K_{dp} to vary between −2 and 10 deg^{-1} similarly to Dolan et al. (2013) and Evaristo et al. (2013). Table 2 lists parameters of the membership functions for the planes $Z_h - Z_{dr}$ and $Z_h - K_{dp}$ in comparison with those used in Baldini et al. (2005).

3.1.3 Graupel IWC estimation

The second important implications of the T-matrix simulations concerns estimation of graupel ice water content. The IWC of graupel (hereinafter $\mathrm{IWC_g}$) computed from the same simulation was related to the simulated Z_h by means of a power law relation of the form

$$\mathrm{IWC_g} = aZ_h^b \tag{2}$$

where $a = 4.64 \times 10^{-4}$, $b = 7.12 \times 10^{-1}$ for spheroid graupel and $a = 4.70 \times 10^{-4}$, $b = 6.89 \times 10^{-1}$ for conical graupel; $\mathrm{IWC_g}$ is in $\mathrm{g\,cm^{-3}}$ and Z_h is in $\mathrm{mm^6\,m^{-3}}$. To assess the uncertainty of (2) we considered the normalized standard error (NSE) between the simulated $\mathrm{IWC_g}$ obtained from (1) and the one estimated by (2). NSE was 0.553 for speroidal and 0.523 for conical shapes, respectively. The normalized bias was 0.012

AMTD
8, 9241–9287, 2015

for spheroidal and 0.005 for conical shapes, respectively, indicating that (2) is unbiased. Since the coefficients of (2) for the two shapes of graupel were very similar, we simply used those found for spheroid graupel for both graupel shapes. When applied to conical graupel, the NSE changed by less than 6 %.

3.1.4 Radar data processing

The basic steps listed below are applied to radar data for the considered events.

- Selection of volumes which present 8 complete PPIs at the 14 elevation angles and total LINET strokes (CG and IC) were detected within five minutes of each radar volume scan in the 120 km area radar coverage.
- Estimation of 0 °C level using vertical profiling of LIRE soundings for each day.
- Estimation of K_{dp} from Φ_{dp} using finite difference method (Bringi and Chandrasekar, 2001)
- Attenuation correction for Z_h and Z_{dr} using linear relation of K_{dp} with specific attenuation and specific linear attenuation.
- Resampling of polarimetric measurements at 1200 m of range resolution (16 range bins).
- Detection of graupel using the FL HCA for C-band optimized for graupel
- Estimation of columnar IWC_g by integrating in the vertical the IWC_g derived from (2) for each radar sampled volume classified as graupel in the region that typically consists of negative charging zone (vertical extension between −40° and 0°), i.e. the column of graupel above the 0° level.
- Estimation of IWCg beyond 25 km from the Polar 55C radar to detect cells above the ML and to avoid underestimation due to the cone of silence in the vicinity of the radar.

AMTD
8, 9241–9287, 2015

– Calculation of Total Amount of Graupel (TAG, in kg) by integrating the columnar IWC_g over the radar resolution volumes (i.e., all values of columnar IWC were summed and multiplied by the total area of the corresponding radar bin) classified as graupel.

3.2 2-D video disdrometer processing

The 2-DVD data were filtered to remove spurious drops due to splashing or wind effect (Tokay et al., 2001). This resulted in removing 14 % of the 2.2×10^6 drops collected during SOP1.1. Then, the observed diameters were partitioned into 50 bins with a constant width of 0.2 mm. Ten drops in each 1 min spectra were requested to classify a spectrum as rain. A total of 4761 1 min RSDs were obtained.

Techniques for partitioning rain into stratiform or convective from point-wise disdrometer measurements collected at ground can be considered as either those based on properties of rain rate time series, such as intensity and time variability (e.g., Bringi et al., 2003; Marzano et al., 2010) or those based on RSD parameters (e.g., Bringi et al., 2009). In this study, the technique of Bringi et al. (2009) was reformulated to apply it to both radar measurements and disdrometer data, the latter converted into dual-polarization radar measurements via T-matrix scattering computations. Simulations were performed with the following assumptions: temperature of 20 °C, the shape-size model of Beard and Chuang (1987) and zero-mean Gaussian canting angle distribution with standard deviation of 7.5°. The 1 min RSDs were classified as stratiform or convective using criteria of Bringi et al. (2009) based on N_w (i.e., the normalized intercept parameter) and D_o. Representing corresponding radar measurements a specific frequency in the two-dimensional space defined by Z_h and Z_{dr} allows to identify different precipitation regimes. Measurements collected by 2-DVD from 12 September to 12 November 2012 were analyzed at different bands (not shown). A threshold has been identified for C-band to partition the $Z_h - Z_{dr}$ plane into stratiform and convective regions (herein after C/S threshold) as $Z_h = 36.86 + 0.8405 Z_{dr}$, where Z_{dr} is in dB and

AMTD
8, 9241–9287, 2015

Z_h in dBZ. The results of the classification and their relation with other measurements available are presented and discussed in Sect. 5.2.

4 Dataset description

Eleven convective precipitation events were selected, in which both radar and lightning measurements were available (from 3 September 2012 to 6 November 2012, while 2-DVD measurements over Sapienza site were continuously available from 12 September 2012 to 12 November 2012). Six of these events were considered as Intense Observing Period (IOP). The 2-DVD detected 4761 min of rain: the 93.3 % of these was classified stratiform and the 6.7 % was classified convective. Events with the highest percentage of convective minutes were 13 September, 12 and 15 October 2012, when 10.2, 15.6 and 28.6 % of minutes were classified as convective, respectively. The total number of strokes recorded in 24 h were 3621, 7011 and 3388 for the 13 September, 12 and 15 October, respectively (Table 3). These three events, corresponding to three IOPs, were those with the most intense precipitation and will be described in details both from synoptic side and from observations side.

4.1 13 September 2012 case study

This case occurred during the IOP2 (12–13 September 2012) that mainly involved North East Italy and Liguria-Tuscany site, while intense precipitation occurred also in CI. During the morning of 12 September a cold front extending from northern Germany to northern Alps occurred. Associated trough moved toward Italy and then evolved into a cut-off between Corsica and CI in the afternoon of 13 September. Main rainfall activity were located more to the south-east (Naples area), while scattered deep convection occurred over the CI site.

Radar data collected by the Polar 55C during the event were used to monitor the evolution of the convective activity while satellite images gives a more extended view

AMTD
8, 9241–9287, 2015

of the development the events. Figure 2a–c, show PPIs of horizontal equivalent reflectivity factor collected by the Polar 55C at a 1.6° elevation angle during three phases of the precipitation event. A maximum radar range of 120 km was used. LINET strokes are also shown over radar observation. At 20:00 UTC at 80 km South the Polar 55C the initial stage of a convective cell (high reflectivity restrict area with few strokes superimposed) is found. One hour later, this cell was developed and covered larger high reflectivity area superimposed by thirty strokes detected, while at 22:30 UTC this cell split in a number of cells covering a wide area, moving southerly away from radar. Coincident MSG images at 10.8 µm are shown in Fig. 2e–g. The LINET strokes superimposed reveal that the intense convective system developed over the Tyrrhenian Sea. The portion of the system observed by Polar 55C after 20:00 UTC moves and extends easterly over the sea. MSG brightness temperature values associated to the position of strokes are around −50 °C indicating that the height of the top of cloud reach about 10 km from ground.

4.2 12 October 2012 case study

This event occurred during IOP12a carried heavy precipitation from 11 till 12 October 2012 over the CI site, mainly along Lazio and Umbria, associated with a secondary trough over Central Mediterranean sea. The rainfall amount reached more than 150 mm in six hours. This event started over the Tyrrhenian Sea, where several MCSs (Mesoscale Convective System) developed during night between 11 and 12 October. The convective systems reached the Central Italy in the early morning of 12 October, causing heavy precipitations over Northern part of Lazio and Umbria regions. Rain was not persistent, but achieved maxima of 140–160 mm in a few hours. Polar 55C partially observed this event, which significantly developed outside of radar coverage as shown in MSG images (Fig. 3d–f). At 04:30 UTC the most intense part of the event, in which LINET strokes are detected occurred over Tyrrhenian Sea, was located southwesterly respect to the radar. Polar 55C (Fig. 3a–c) was able to observe just half of the MCS

AMTD
8, 9241–9287, 2015

occurred at 0430 (that was the third of the event) and at over 80 km of distance. One hour and half later, the MCS moves southerly and more distant from radar (100 km).

4.3 15 October 2012 case study

This case study belongs to IOP 13, which took place on 14 and 15 October 2012 across a vast area in the western Mediterranean including also all three hydro-meteorological focus sites in Italy. On these days, a severe weather warning was issued for central Italy, particularly for Rome, by some weather services. The precipitation event was associated with a trough that deepened significantly over the northern Tyrrhenian Sea that pushed a frontal system eastward which advected moist air from Tyrrhenian Sea inland to fuel deep convection on the Tyrrhenian coast, west of Rome. The synoptic-scale system moved rapidly to the east and triggered a line of convection that crossed the western half of Central Italy from north to south within a few hours (Ferretti et al., 2014; Federico et al., 2014). Most of the precipitation produced by this system occurred in the late afternoon of 15 October across the western part of CI and on the western slopes of the Apennines. The total rainfall amount recorded in Rome was weaker than predicted – the highest daily amount recorded within the historic area of Rome was 35 mm by the operational rain gauge in Eleniano (close to Sapienza site). A maximum rainfall rate of 124 mm h^{-1} was recorded by the Sapienza 2-DVD at 18:09 UTC. Three phases of the precipitation event are shown by the PPIs of Z_h in Fig. 4a–c. At 16:00 UTC a few convective cells were detected by Polar 55C northwest of Rome (Fig. 4a) while the lightning activity within the radar coverage area was low (11 strokes detected by LINET in five minutes). By 17:30 UTC, a line of convective cells with radar reflectivity greater than 50 dBZ was formed and the lightning activity became more intense (Fig. 4b). During a five-minute interval around this time, LINET detected 227 strokes within the radar coverage area, costly co-located with the area of higher radar reflectivity (Fig. 4b). The convective activity weakened after 19:00 UTC (Fig. 4c), and most of precipitation detected by the radar exhibited stratiform characteristics, especially over Rome, while the lightning activity had drastically decreased (37 strokes were recorded in five minutes

AMTD
8, 9241–9287, 2015

over the radar coverage area). MSG images overlapped by strokes (Fig. 4d–f) confirm that the most intense phase of development of the line of convection occurred within the radar area coverage.

5 Results

5.1 Dual polarization radar analysis and lightning activity

The RHIs collected by Polar 55C along the azimuth of the Sapienza site (293°) during intense precipitation enabled us to examine the behavior of the FL-based HCA and IWC_g estimation. An example of the classification output from the RHI at 17:55 UTC is shown in Fig. 5a. For this RHI, radar measurements were resampled to a range resolution of 300 m and hydrometeor classes identified by the HCA are *rain*, *dry snow*, *wet snow*, *graupel* and *small hail*, *hail* and *a mix of rain and hail*. Two intense convective cells were present around 12 and 25 km from the radar and near Rome at 17:55 UTC. The closest one was characterized by the presence of graupel from the ground to a height of 8 km, while also the second one was characterized by graupel up to 6 km, as well as hail, and hail-mixed with other hydrometeors, which were present closer also to the ground. These cells mostly had Z_h values of 40 dBZ, reaching 50 and 55 dBZ in the cores of the cells. Comparing these RHI classification results with those obtained with (Baldini et al., 2005), the new scheme adds the 8 % of pixels classified as graupel. Figure 5b shows the columnar IWCg (in $kg\,m^2$) for each range bin for the two classification schemes. The new scheme estimates more columnar IWC_g (from 2 to 10 %) along the range distance. At this time (integrating measurements in 2 min) the LINET detected 18 lightning strokes within a 10 km radius from the peaks in columnar IWCg. Although the RHI scanning mode provides better vertical resolution than radar PPI volume scans, the RHI measurements cover a very narrow azimuthal slice (i.e., only the 1° beam width), which makes it difficult to relate the estimated graupel mass content to the lightning occurring across a wider horizontal area. Therefore, volume

AMTD
8, 9241–9287, 2015

scans processed as described in Sect. 3.1.4 were used to consider the entire 120 km radar coverage area and to have data every five minutes.

To investigate the relationship between the ice mass and lightning activity, the columnar IWC_g was calculated for nearly the entire radar coverage area and compared with the number of strokes (CG and IC) detected by the LINET. Figure 6 shows an example of columnar IWC_g in three PPI scans of 15 October. We found the relative peaks in lightning activity tended to follow peaks in columnar IWC_g (Fig. 6). Figure 6a shows that columnar IWC_g was less than $3\,kg\,m^{-2}$ during the initial stage of the event at 16:00 UTC when only a few coincident strokes were detected, which indicated early convective development in the radar area coverage. At 17:30 UTC (Fig. 6b) the line of cells oriented northeast to southwest were characterized by high values of columnar IWC_g (up to $5\,kg\,m^{-2}$) and a high number of lightning strokes whose locations were coincident with this line of convective cells. Figure 6c shows the columnar IWC_g at 19:20 UTC, by which time convection had weakened and there was little of it found across the northwestern part of Rome. Just a few lightning strokes and low columnar IWC_g were found at southeast of Rome.

A quantitative relationship between the total number of LINET strokes (both CG and IC) and the TAG was determined. Figure 7 shows the scatter plot between TAG and the total number of LINET strokes in the coverage area of the Polar 55C for the three case studies (different colors are used for each case study). A good linear correlation was found for the two case studies occurred in October while for the case of 13 September a less correlation was found (Table 4). Furthermore, for all cases a higher correlation (higer values of R^2) between TAG and strokes are obtained when the graupel hydrometeors are detected by the new HCA (Table 4). Observing the scatter plot in Fig. 7 two different beahaviours appear well defined, one related to 15 October, and one to 13 September and 12 October. The slopes of linear regression for the latter two dates are very similar and the TAG for these cases is understimated around the 70 % if fit to 15 October is used. The threshold found by Formenton et al. (2014) using model results, converted in TAG and flash rate in 5 min (multiplying the columnar IWC_g for the mean

AMTD
8, 9241–9287, 2015

of graupel estension in m^2 detected by Polar 55C) is in good agreement with the fitting line of 15 October. Observations confirm model results highlighting a linear relationship between the number of lightning strokes and graupel mass (TAG). However, for the 13 September and 12 October this linear relationship has a lower slope, i.e. the mass of graupel estimated produce more strokes than expected by model outputs. Different causes could contribute to this fact and can be related to (i) radar measurement geometry and to (ii) type of convective event. Concerning (i) precipitation patterns observed by radar for the three events, present areas of intense precipitation at different distances from Polar 55C. In particular, on 13 September and 12 October, such areas, where graupel was also found, were prevalently farther 80 km (the mode of distance of peak of IWC_g was located over 70 km from radar as shown in the last column of Table 3). At such distance radar beam becomes very wide (1 ° of beamwidth corresponds to a sample volume of about 1.8 km height at 80 km) that implies that backscattering is generated by more inhomogeneous volume of hydrometeors with respect to that from closer, smaller and more homogenous sampled volume, inducing possible misdetection of graupel from HCA. For both cases, Polar 55C is able to observe the tail of the core of the MCS that is located over the Tyrrhenian Sea (see Figs. 2 and 3). Another source of underestimation of graupel column by radar can be attributed at difference in height of 0° isothermal estimated by radiosounding. For the 15 October 2012 it was estimated at about 2.9 km, while for the other two cases it was above 3.4 km (Table 3). Since the column of graupel is calculated above the 0° level, the more high this level is, the more the height of the column is reduced. In order to quantify this reducing, we have performed some simulation, supposing a homogeneous graupel column height 6 km from ground. Comparing different heights of 0° level that were detected during the events analysed, the graupel column can be reduced up to 17 % for a height of 3.4 km and up to 30 % for a height of 3.9 km respect to 2.9 km of 0° level height. These explanations lead us to think that the case of 15 October 2012 was observed by a radar in a better conditions of observations than the other two. Concerning the causes (ii) the electrification process links the microphysical and kinematic evolution

AMTD
8, 9241–9287, 2015

of storms with the evolving characteristics of storm charge and lightning. Storms with a large updraft mass flux and large graupel volume typically produce large flash rates (e.g., Wiens et al., 2005; Deierling and Petersen, 2008). According to the non-inductive charging mechanism (see Saunder et al., 1993), graupel is only one ingredient required for charge generation in clouds. The other key feature is the size and strength of the updraft (e.g., Deierling and Petersen, 2008). The total lightning flash rate (IC + CG) is tied to the flux of hydrometers within the cloud (Blyth et al., 2001; Latham et al., 2004; Weins et al., 2005; Deierling et al., 2008). More specifically, the downward flux of graupel through a region of significant updraft ($> 5\,\mathrm{m\,s^{-1}}$) that occupies altitudes where ice crystals and super-cooled droplets coexist ($-5 < T < -40\,^{\circ}\mathrm{C}$) regulates the total flash rate. So with all that said, we cannot solely use graupel IWC to fully explain the differences in flash rate amongst the 3 case studies. Considering the flux hypothesis (Blyth et al., 2001; Latham et al., 2004), we can say that the differences in graupel IWC for a similar total number of strokes detected by LINET (Fig. 7) suggest there were differences in the updraft characteristics between the two type of events. For the 15 October event (magenta dots in Fig. 7) that had the most graupel present, the updraft need not be as strong or large through the charging zone (i.e., $-5 < T < -30\,^{\circ}\mathrm{C}$) as the other events to produce the similarly observed lightning activity. Since there was less graupel present for the 12 October (or 13 September) event, a stronger/larger updraft through the charging zone was required to produce similar lightning activity as 15 October. However, measurements of the updraft at altitudes above $-5\,^{\circ}\mathrm{C}$ (not available from ground instruments deployed during SOP1.1 in CI) would be required to validate such conclusions.

Although different regimes were found in the relation between TAG and the number of strokes, the rather good linear fit provide a quantitative means for evaluating the number of lightning strokes based upon the cloud ice mass due to graupel quantified as TAG in kg. In particular, the relation for the case of 15 October is in good agreement with model results, supporting the hypothesis that measurements were taken in optimal conditions respect to the radar geometry of acquisition. This important finding could be

AMTD
8, 9241–9287, 2015

exploited for applications involving lightning data simulation and/or assimilation in NWP models in order to improve the forecast of the convection (Lynn et al., 2012; Federico et al., 2014).

Finally, the ability of the LINET network to discriminate between CG and IC strokes, and to determine the polarity associated with CG strokes, was analyzed. Severe storms appeared to be significant producers of +CG lightning (Carey and Rutledege, 2003). Among the three case studies analysed, on the 15 October 2012 the 30 % of CG were positive, while for the other two case studies +CG were around 20 %. Considering the relation between TAG, and IC, +CG and -CG results are summarized in Table 5 for the 15 October case study. Most of the strokes detected were −CG and they increased with increasing of TAG (linear regression yields an $R^2 = 0.73$), but the number of the IC strokes detected was lower and more poorly correlated with TAG ($R^2 = 0.48$). This suggests that the IC strokes are not well correlated to the graupel aloft but could be better correlated with other hydrometeors such as with the presence of hail at the surface (Cummins et al., 2000). However, it is worth noting that the LINET network detects more CG than IC strokes, and the lower correlation could also be due to the large baseline between sensors near the coast (Zinner et al., 2013), which can cause a reduced detection efficiency and significant impact on the detection of weak ICs. Since the best correlation was found for the −CG, the time evolution of the graupel total mass and −CG was examined (Fig. 8). The increasing and decreasing trends of CG lightning activity tended to follow that of the total mass of graupel, which agrees with the findings of Lopez et al. (1997).

Some general considerations can be obtained from the results shown: (i) the linear correlation between TAG and the number of strokes (total and −CG) confirms the theory for which the amount of graupel aloft, often associated to the negative charge in the clouds (Saunders, 1993) is directly related to the mechanism of lightning production, and (ii) the modelling results of Formenton et al. (2013), in which there exists a minimum threshold of columnar IWC required to produce lightning and this threshold

AMTD
8, 9241–9287, 2015

increases with the enhancement of electrical activity, is confirmed by radar observations of 15 October.

5.2 Multi-sensor analysis over Sapienza site

The 4761 1 min RSDs RSDs were classified as stratiform and convective using the criterion described in Sect. 3.2 and compared with radar measurements observed over Sapienza site for all the dataset. Furthermore, their relation with lightning activity was assessed focusing on the 15 October 2012 case. The scatter plot $Z_h - Z_{dr}$ computed for all the 1 min RSD is shown in Fig. 9 in which the threshold for separating convective from stratiform regimes is plotted in black line. Superimposed are the Polar 55C radar reflectivity and differential reflectivity (coloured circles) measured at a 1.6 ° elevation angle and averaged over 4 consecutive 75 m range bins above the Sapienza site. A C/S classification method based on the detection of the melting layer signature corresponding to the standard deviation of Z_{dr} (Baldini and Gorgucci, 2006) was adopted. It worth noting that the most of stratiform minutes are below the C/S threshold detected by 2-DVD and some of these (7.5 %) are just above, around the threshold. Six convective minutes are detected by Polar 55C and one of these is found just below the C/S threshold. Results confirm that radar classification are in fairly good agreements with the C/S threshold.

The RSD averages over the convective minutes of the three cases are shown in Fig. 10. The shape of lines of 13 September and the 12 October are very similar, while concerning the 15 October the concentration of larger drops ($D > 3$ mm) is greater than the other two cases. This different behaviour highlights different type of convective precipitation events (more precisely, this concerns the part of the event occurring over Rome). In fact, on 15 October, the event observed in Rome was a more intense than the other two, and also characterized by more intense lightning activity: 156 strokes were detected by LINET in 1 min and within 10 km of the Sapienza site the 15 October, while 43 and 7 strokes were measured the 13 September and 12 October, respectively.

AMTD
8, 9241–9287, 2015

For this reason, further analysis involving LINET and 2-DVD will focus only on the 15 October case study. For this case, the time series of 1 min radar reflectivity factor simulated from the 188 RSDs compared with that measured by the Polar 55C radar are shown in Fig. 11. In addition, the resultant convective-stratiform classification and the lightning activity (within 10 km of the Sapienza site) is also shown. The C/S classification using 2-DVD threshold applied to the radar measurements was in agreement with the classification from the disdrometer measurements. Between 17:50 and 18:20 UTC a large number of strokes were detected by LINET, when rain was classified as "convective". However, convective rain was also found before 17:00 UTC, but just one stroke was detected at that time. Before 17:00 UTC there may not have been sufficient graupel aloft to produce lightning (Formenton et al., 2013). Between 16:50 and 17:00 UTC, the rain at Sapienza was classified as stratiform, but at that time there were lightning strokes due to convective cells containing graupel detected by radar in the vicinity. Furthermore, no graupel was detected by the Polar 55C at this time, which agrees with the presence of stratiform rain there. The most intense precipitation was detected between 1743 until 19:09 UTC, that includes the most intense lightning activity. Radar reflectivity factor exhibited two peaks during the convective rain, separated by a few minutes classified as stratiform rain around 18:00 UTC (Fig. 10). This trend and the C/S classification agreed with that found from the RHI in Fig. 5a, where two consecutive, intense convective cells spatially separated by a region of uniform hydrometeors (i.e., similar to the bright band present in stratiform precipitation) were detected by the FL classifier. Lightning activity at the Sapienza site ended by 18:25 UTC, and afterwards, all rain that fell there was classified as stratiform. The relationship between different phases of cloud (liquid and solid) and the lightning activity over the Sapienza site is found in the contingency tables concerning the 15 October case study (Table 6). Stratiform events calculated using 2-DVD threshold (Table 6a) and the absence of graupel ($IWC_g = 0$) (Table 6b) are in good agreements with the absence of LINET strokes. Statistic scores comparing convective minutes-strokes (Table 6a) and graupel presence-strokes (Table 6b) were calculated. Higher Probably Of Detection (POD) and

AMTD
8, 9241–9287, 2015

Equitable Threat Score (ETS) and lower False Alarm Rate (FAR) are found to be better for Table 6b (POD = 0.85; FAR = 0.25, ETS = 0.64) than for Table 6a (POD = 0.64; FAR = 0.51; ETS = 0.29), indicating that the ice phase of cloud is more in agreement with lightning activity than liquid phase.

6 Summary and conclusions

Convective events occurred during the HyMeX SOP 1.1 in the CI HyMeX hyrometeorological site, and in particular within the Polar55 C coverage area, were investigated using observations from three complementary instruments, namely the LINET lightning network, a dual-polarization C-band weather radar, and a 2-D video disdrometer. Measurements from the LINET network provided the common framework to interpret different signatures of convection detected by the other instruments and to relate them to lightning activity. The disdrometer, installed 14 km away from the dual-polarization radar, provided estimates of raindrop size distribution at ground whereas, data from the scanning dual-polarization C-band radar were used to analyze important cloud processes related to convection on a wider portion of space. In particular, radar scans at constant azimuths and variable elevations (RHIs) are used to detect the vertical fine structure of convective cells with the support of a fuzzy logic hydrometeor classification system, properly tuned for C-band measurements and for graupel detection. Data from volume scanning regularly repeated every 5 min, have been used to highlight the relationship between lightning activity (expressed by the number of strokes detected by LINET) and the amount of graupel, whose presence in a radar resolution volume is revealed by the hydrometeor classification algorithm. Using T-matrix simulations results, we formulated a power–law relation to obtain graupel IWC from radar reflectivity in order to examine impact of the total mass of graupel on the number of LINET strokes. Among three important case studies were selected, that of 15 October exhibited a linear relation between total mass of graupel and number of LINET strokes, with a high coefficient of determination (R^2 = 0.856) and a slope in agreement with

AMTD
8, 9241–9287, 2015

model results. This relationship can be considered an important step towards quantifying the microphysical mechanisms that play a role in lightning activity. In the other events, a linear relation was still found, but with a slope smaller than that found for the case of 15 October, and, consequently, from the slope compliant with the Formenton et al. (2013) model. The fact that these events developed over the sea and far from the radar (more farther than 80 km) suggests also an influence of observation geometry. While the flux hypothesis suggest that there were differences in the updraft characteristics between the events. However, more observations, beyond the HyMeX SOP 1.1, should be performed in order to establish whether a unique strokes-IWC_g relations exists, although geometry of observation and discrimination capabilities of dual-polarization radar can limit these investigations.

To assess the impact of lightning activity on the raindrop size distribution at ground, we partitioned the 2-DVD measured spectra into stratiform or convective classes and tested the classification against polarimetric radar measurements and the number of lightning strokes detected by LINET. Comparison with classification method based on polarimetric radar measurements showed a fairly good agreement in particular for the detection of the stratiform part. It was found that a large number of strokes were detected by LINET, when rain was classified as "convective" (between 17:50 and 18:20 UTC). Nevertheless, convective rain was also found before (17:00 UTC), with few strokes detected. This fact can be explained by the low amount of graupel aloft as detected from radar measurements. High performance from statistical scores were obtained from presence of graupel in relation to occurrence of LINET strokes. However, lightning activity was not always found when the precipitation regime was classified as convective. In fact, a certain quantity of graupel aloft is needed to produce strokes although characteristics for convective rain are observed at ground.

Acknowledgements. This research has been carried out as a contribution to the SOP 1 of the HyMeX program. The setup of instruments for HyMeX SOP 1.1 in the CI area, was possible thanks to a synergy between Italian Institutions (CETEMPS-University of L'Aquila, ISAC-CNR, DIET-Sapienza University of Rome, University of Ferrara), NASA-GSFC, and the HyMeX coor-

AMTD
8, 9241–9287, 2015

dination. Authors thanks Angelo Viola, Stefania Argentini, Ilaria Pietroni e Giampietro Casasanta for providing and processing SODAR data. The authors also acknowledge the NASA Global Precipitation Measurement (GPM) mission ground validation program under the direction of Matthew Schwaller and Walter A. Petersen, GPM ground validation and science manager, respectively, for providing instruments and expertise, and Arthur Hou, former GPM project scientist (deceased) who promoted the participation of NASA to this campaign.

References

Albrecht, R., Morales, C., and Dias, M.: Electrification of precipitating systems over the Amazon: physical processes of thunderstorm development, J. Geophys. Res., 116, D08209, doi:10.1029/2010JD014756, 2011.

Baldini, L. and Gorgucci, E.: Identification of the melting layer through dual-polarization radar measurements at vertical incidence, J. Atmos. Ocean. Tech., 23, 829–839, 2006.

Baldini, L., Gorgucci, E., Chandrasekar, V., and Petersen, W. A.: Implementations of CSU hydrometeor classification scheme for C-band polarimetric radars, in: Preprints, 32nd Conf. on Radar Meteorology, Albuquerque, NM, 22–28 October 2005, Amer. Meteor. Soc., 95865, available at: https://ams.confex.com/ams/pdfpapers/95865.pdf (last access: 29 August 2015), 2005.

Baldini, L., Roberto, N., Gorgucci, E., Fritz, J., and Chandrasekar, V.: Analysis of dual polarization images of precipitating clouds collected by the COSMO SkyMed constellation, Atmos. Res., 144, 21–37, doi:10.1016/j.atmosres.2013.05.010, 2014.

Barber, P. and Yeh, C.: Scattering of electromagnetic waves by arbitrarily shaped dielectric bodies, Appl. Optics, 14, 2864–2872, 1975.

Beard, K. V. and Chuang, C.: A new model for the equilibrium shapes of raindrops, J. Atmos. Sci., 44, 1509–1524, 1987.

Betz, H.-D., Schmidt, K., Laroche, P., Blanche, P., Oettinger, W. P., Defer, E., Dziewit, Z., and Konarski, J.: LINET – an international lightning detection network in Europe, Atmos. Res., 91, 564–573, 2009.

Blyth, A. M., Christian, H. J., Driscoll, K., Gadian, A. M., and Latham, J.: Determination of ice precipitation rates and thunderstorm anvil ice contents from satellite observations of lightning, Atmos. Res., 59–60, 217–229, 2001.

AMTD
8, 9241–9287, 2015

Bringi, V. N. and Chandrasekar, V.: Polarimetric Doppler Weather Radar, Cambridge Univ. Press., Cambridge, UK, 2001.
Bringi, V. N., Chandrasekar, V., Hubbert, J., Gorgucci, E., Randeu, W. L., and Schoenhuber, M.: Raindrop size distribution in different climatic regimes from disdrometer and dual-polarized radar analysis, J. Atmos. Sci., 60, 354–365, 2003.
Bringi, V. N., Williams, C. R., Thurai, M., and May, P. T.: Using dual-polarized radar and dual-frequency profiler for DSD characterization: a case study from Darwin, Australia, J. Atmos. Ocean. Tech., 26, 2107–2122, 2009.
Carey, L. D. and Rutledge, S. A.: A multiparameter radar case study of the microphysical and kinematic evolution of a lightning producing storm, Meteorol. Atmos. Phys., 59, 33–64, 1996.
Carey, L. D. and Rutledge, S. A.: The relationship between precipitation and lightning in tropical island convection: A C-band polarimetric radar study: a C-band polarimetric radar study, Mon. Weather Rev., 128, 2687–2710, 2000.
Carey, L. D. and Rutledge, S. A.: Characteristics of cloud-to-ground lightning in severe and nonsevere storms over the central United States from 1989–1998, J. Geophys. Res., 108, 4483, doi:10.1029/2002JD002951, 2003.
Cummins, K. L., Murphy, M. J., and Tuel, J. V.: Lightning detection methods and meteorological applications, in: Proc. of the IV International Symposium on Military Meteorology, Malbork, Poland, 25–28 September 2000.
Deierling, W. and Petersen, W. A.: Total lightning activity as an indicator of updraft characteristics, J. Geophys. Res., 113, D16210, doi:10.1029/2007JD009598, 2008.
Deierling, W., Petersen, W. A., Latham, J., Ellis, S., and Christian, H. J.: The relationship between lightning activity and ice fluxes in thunderstorms, J. Geophys. Res., 113, D15210, doi:10.1029/2007JD009700, 2008.
Dolan, B. and Rutledge, S. A.: A theory-based hydrometeor identification algorithm for X-band polarimetric radars, J. Atmos. Ocean. Tech., 26, 2071–2088, 2009.
Dolan, B., Rutledge, S. A., Lim, S., Chandrasekar, V., and Thurai, M.: A robust C-band hydrometeor identification algorithm and application to a long-term polarimetric radar dataset, J. Appl. Meteorol. Clim., 52, 2162–2186, 2013.
Ducrocq, V., Braud, I., Davolio, S., Ferretti, R., Flamant, C., Jansa, A., Kalthoff, N., Richard, E., Taupier-Letage I., Ayral, P. A., Belamari, S., Berne, A., Borga, M., Boudevillain B., Bock O., Boichard, J. L., Bouin, M. N., Bousquet, O., Bouvier, C., Chiggiato, J., Cimini, D., Corsmeier, U., Coppola, L., Cocquerez, P., Defer, E., Delanoe, J., Girolamo, P. D., Doerenbecher, A.,

AMTD
8, 9241–9287, 2015

Drobinski, P., Dufournet, Y., Fourrie, N., Gourley, J.J., Labatut, L., Lambert, D., Le Coz, J., Marzano F. S., Molinie, G., Montani, A., Nord, G., Nuret, M., Ramage, K., Rison, B., Roussot, O., Said, F., Schwarzenboeck, A., Testor, P., Baelen, J. V., Vincendon, B., Aran, M., and Tamayo, J.: HyMeX-SOP 1, the field campaign dedicated to heavy precipitation and flash flooding in the northwestern Mediterranean, B. Am. Meteorol. Soc., 95, 1083–1100, 2014.

Evaristo, R., Bals-Elsholz, T. M., Williams, E. R., Smalley, D. J., Donovan, M. F., and Fenn, A.: Relationship of graupel shape to differential reflectivity: theory and observations, in: Proceedings, 93rd Amer. Meteor. Soc. Annual Meeting, Austin, TX, 5–10 January 2013, Amer. Meteor. Soc., 1–9, available at: https://ams.confex.com/ams/93Annual/webprogram/Paper214462.html (last access: 29 August 2015), 2013.

Federico, S., Avolio, E., Petracca, M., Panegrossi, G., Sanò, P., Casella, D., and Dietrich, S.: Simulating lightning into the RAMS model: implementation and preliminary results, Nat. Hazards Earth Syst. Sci., 14, 2933–2950, doi:10.5194/nhess-14-2933-2014, 2014.

Ferretti, R., Pichelli, E., Gentile, S., Maiello, I., Cimini, D., Davolio, S., Miglietta, M. M., Panegrossi, G., Baldini, L., Pasi, F., Marzano, F. S., Zinzi, A., Mariani, S., Casaioli, M., Bartolini, G., Loglisci, N., Montani, A., Marsigli, C., Manzato, A., Pucillo, A., Ferrario, M. E., Colaiuda, V., and Rotunno, R.: Overview of the first HyMeX Special Observation Period over Italy: observations and model results, Hydrol. Earth Syst. Sci., 18, 1953–1977, doi:10.5194/hess-18-1953-2014, 2014.

Formenton, M., Panegrossi, G., Casella, D., Dietrich, S., Mugnai, A., Sanò, P., Di Paola, F., Betz, H.-D., Price, C., and Yair, Y.: Using a cloud electrification model to study relationships between lightning activity and cloud microphysical structure, Nat. Hazards Earth Syst. Sci., 13, 1085–1104, doi:10.5194/nhess-13-1085-2013, 2013.

Friedrich, K., Kalina, E. A., Masters, F. J., and Lopez, C. R.: Drop-size distributions in thunderstorms measured by optical disdrometers during VORTEX2, Mon. Weather Rev., 141, 1182–1203, 2013.

Gatlin, P. N. and Goodman, S. J.: A total lightning trending algorithm to identify severe thunderstorms, J. Atmos. Ocean. Tech., 27, 3–22, 2010.

Goodman, S. J., Buechler, D. E., and Wright, P. D.: Polarization radar and electrical observations of microburst producing storms during COHMEX, in: AMS 24th Conference on Radar Meteorology, Tallahassee FL, 27–31 March 1989, 59/141, 1989.

Heymsfield, A.: Ice crystal terminal velocities, J. Atmos Sci., 29, 1348–1357, 1972.

AMTD
8, 9241–9287, 2015

Lagouvardos, K., Kotroni, V., Defer, E., and Bousquet, O.: Study of a heavy precipitation event over southern France, in the frame of HYMEX project: observational analysis and model results using assimilation of lightning, Atmos. Res., 134, 45–55, doi:10.1016/j.atmosres.2013.07.003, 2013.

Lang, T. J. and Rutledge, S. A.: Relationships between convective storm kinematics, precipitation, and lightning, Mon. Weather Rev., 130, 2492– 2506, 2002.

Lang, S., Tao, W.-K., Simpson, J., and Ferrier, B.: Modeling of convective-stratiform precipitation processes: sensitivity to partitioning methods, J. Appl. Meteorol., 42, 505–527, 2003.

Latham, J., Blyth, A. M., Christian Jr., J. H., Deierling, W., and Gadian, A. M.: Determination of precipitation rates and yields from lightning measurements, J. Hydrol., 288, 13–19, 2004.

Latham, J., Petersen, W. A., Deierling, W., and Christian Jr., H. J.: Field identification of a unique globally dominant mechanism of thunderstorm electrification, Q. J. Roy. Meteor. Soc., 133, 1453–1457, 2007.

Lim, S., Chandrasekar, V., and Bringi, V. N.: Hydrometeor classification system using dual-polarization radar measurements: model improvements and in situ verification, IEEE T. Geosci. Remote, 43, 792–801, 2005.

Liu, H. and Chandrasekar, V.: Classification of hydrometeor based on polarimetric radar measurements: development of fuzzy logic and neuro-fuzzy systems and in situ verification, J. Atmos. Ocean. Tech., 17, 140–164, 2000.

López, R. E. and Aubagnac, J. P.: The lightning activity of a hailstorm as a function of changes in its microphysical characteristics inferred from polarimetric radar observations, J. Geophys. Res., 102, 16799–16813, doi:10.1029/97JD00645, 1997.

Lynn, B., Yair, Y., Price, C., Kelman, G., and Clark, A. J.: Predicting cloud-to-ground and intracloud lightning in weather forecast models, Weather Forecast., 27, 1470–1488, doi:10.1175/WAF-D-11-00144.1, 2012.

Machado, L. A. T., Silva Dias, M. A. F., Morales, C., Fisch, G., Vila, D., Albrecht, R., Goodman, S.J., Calheiros, A. J. P., Biscaro T, Kummerow C., Cohen, J., Fitzjarrald, D., Nascimento, E., Sakamoto, M., Cunningham, C., Chaboureau, J. P., Petersen, W. A., Adams, D., Baldini, L., Angelis, C. F., Sapucci, L. F., Salio P, Barbosa, H. M. J., Landulfo, E., Souza, R.F., Blakeslee, R.J., Bailey, J., Freitas, S., Lima, W. F., and Tokay, A.: The CHUVA Project – how does convection vary across Brazil?, B. Am. Meteorol. Soc., 95, 1365–1380, 2013.

AMTD
8, 9241–9287, 2015

Marzano, F. S., Cimini, D., and Montopoli, M.: Investigating precipitation microphysics using ground-based microwave remote sensors and disdrometer data, Atmos. Res., 97, 583–600, 2010.
Melani, S., Pasi, F., Gozzini, B., and Ortolani, A.: A four year (2007–2010) analysis of longlasting deep convective systems in the Mediterranean basin, Atmos. Res., 123, 151–166201, 2013.
Miglietta, M. M. and Rotunno, R.: Application of theory to observed cases of orographically forced convective rainfall, Mon. Weather Rev., 140, 3039–3053 2012.
Petersen, W. A. and Jensen, M.: The NASA-GPM and DOE-ARM Midlatitude Continental Convective Clouds Experiment (MC3E). The Earth Observer, vol. 24, issue 1, Earth Observing System Project Science Office, NASA GSFC, Greenbelt, MD, 12–18, available at: http://eospso.gsfc.nasa.gov/sites/default/files/eo_pdfs/Jan_Feb_2012_col_508.pdf (last access: 29 August 2015), 2012.
Petersen, W. A. and Rutledge, S. A.: On the relationship between cloud-to-ground lightning and convective rainfall, J. Geophys. Res., 103, 14025–14040, 1998.
Petersen, W. A., Christian Jr., H. J., and Rutledge, S. A.: TRMM observations of the global relationship between ice water content and lightning, Geophys. Res. Lett., 32, L14819, doi:10.1029/2005GL023236, 2005.
Petracca, M., Casella, D., Dietrich, S., Panegrossi, G., and Sanò, P.: Multisensor atmospheric data mapping system: a web-based graphic tool for multisensor observations of atmospheric data and NWP model forecasts, in: Eumetsat Meteorological Satellite Conference, Vienna, 16–20 September 2013.
Pruppacher, H. R. and Klett, J. D.: Microphysics of Clouds and Precipitation, D. Reidel Publishing Company, 10–73, 1997.
Saunders, C. P. R.: A review of thunderstorm electrification processes, J. Appl. Meteorol., 32, 642–655, 1993.
Schönhuber, M., Lammer, G., and Randeu, W. L.: The 2-D-Video-Distrometer. Precipitation: Advances in Measurement, Estimation and Prediction, edited by: Michaelides, S., Springer, 3–32, 2008.
Sebastianelli, S., Russo, F., Napolitano, F., and Baldini, L.: On precipitation measurements collected by a weather radar and a rain gauge network, Nat. Hazards Earth Syst. Sci., 13, 605–623, doi:10.5194/nhess-13-605-2013, 2013.
Tokay, A., Kruger, W., and Krajewski, J.: Comparison of drop size distribution measurements by impact and optical disdrometers, J. Appl. Meteorol., 40, 2083–2097, 2001.

AMTD
8, 9241–9287, 2015

Tokay, A., Petersen, W. A., Gatlin, P., and Wingo, M.: Comparison of raindrop size distribution measurements by collocated disdrometers, J. Atmos. Ocean. Tech., 30, 1672–1690, 2013.
Wang, P. K.: Mathematical description of the shape of conical hydrometeors, J. Atmos. Sci., 39, 2615–2622, 1982.
Weisman, M. L., Davies, C., Wang, W., Manning, K. W., and Klemp, J. B.: Experiences with 0–36 h explicit convective forecasts with the WRF-ARW model, Weather Forecast., 23, 407–437, 2008.
Wiens, K. C., Rutledge, S. A., and Tessendorf, S. A.: The 29 June 2000 supercell observed during STEPS. Part II: Lightning and charge structure, J. Atmos. Sci., 62, 4151–4177, 2005.
Wu, D., Dong, X., Xi, B., Feng, Z., Kennedy, A., Mullendore, G., Gilmore, M., and Tao, W.-K.: Impacts of microphysical scheme on convective and stratiform characteristics in two high precipitation squall line events, J. Geophys. Res.-Atmos., 118, 11119–11135, 2013.
Zikmunda, J. and Vali, G.: Fall patterns and fall velocities of rimed ice crystals, J. Atmos. Sci., 29, 1334–1347, 1972.
Zinner, T., Forster, C., de Coning, E., and Betz, H.-D.: Validation of the Meteosat storm detection and nowcasting system Cb-TRAM with lightning network data – Europe and South Africa, Atmos. Meas. Tech., 6, 1567–1583, doi:10.5194/amt-6-1567-2013, 2013.

AMTD
8, 9241–9287, 2015

Table 1. Inputs to T-matrix simulations for graupel. Spheroid and conical grauples differ mainly for the axis ratio (b/a) and standard deviation of canting angle (σ).

	Spheroid graupel	Conical graupel
Frequency	5.6 GHz	5.6 GHz
Composition	Mixture of air, ice and water	Mixture of air, ice and water
Fraction of water	Vary ramdomly in [5, 55 %]	Vary ramdomly in [5, 55 %]
Density	Vary ramdomly in [0.2, 0.9] g cm^{-3}	Vary ramdomly in [0.2, 0.9] g cm^{-3}
Temperature	Vary ramdomly in [-15, +5] $^{\circ}$C	Vary ramdomly in [-15, +5] $^{\circ}$C
PSD parameters	Exponential: D_0 [1, 3] logN_0 [2, 3]	Exponential: D_0 [1, 3] logN_0 [2, 3]
b/a	Vary ramdomly in [0.9, 1.0] deg	Vary ramdomly in [0.75, 1.1] deg
σ	Vary ramdomly in [0, 15] deg	Vary ramdomly in [0, 30] deg
Elevation angle	0 $^{\circ}$	0 $^{\circ}$

AMTD
8, 9241–9287, 2015

Table 2. Parameters of beta membership functions (Liu and Chandrasekar, 2000) for C-band and graupel identification (where A is half-width, M is the center, and B is the slope of the beta functions) for $Z_h - Z_{dr}$ and $Z_h - K_{dp}$. Column identified by Opt" referred to functions modified for HCA scheme optimize for graupel identification.

Z_{dr}				Z_{dr}Opt				K_{dp}				K_{dp}Opt			
Z_h	M	A	B	Z_h	M	A	B	Z_h	M	A	B	Z_h	M	A	B
30	0.15	0.65	10	30	0.5	1.5	10	30	−0.15	0.35	10	30	2.5	1.5	10
35	0.25	0.75	10	35	0.5	1.5	10	35	−0.1	0.4	10	35	2.5	2.5	10
40	0.35	0.85	10	40	0.5	1.5	10	40	0.05	0.55	10	40	2.5	3.5	10
45	0.5	1	15	45	0.5	1.5	10	45	0.5	1	15	45	2.5	4.5	10
50	0.75	1.25	15	50	0.5	1.5	10	50	0.75	1.25	15	50	2.5	5.5	10
55	1	1.5	15	55	0.5	1.5	10	55	1	1.5	15	55	2.5	6.5	10

AMTD
8, 9241–9287, 2015

Table 3. Dates for which both radar and LINET data are simultaneosly available. Second and third columns are the HyMeX SOP 1.1 IOP number (in brackets availability of the F20 flights), the Target Area (TA) involved in the IOP. Fourth and fifth columns are the minutes stratiform (/S) and convective (/C) measured by 2-DVD over Sapienza site. Daily number of LINET strokes occurred during Polar55 C observation and in brackets number of strokes in 24 h are shown in sixth column. Seventh column shows height of 0 °C level in m and the last column shows the mode of the distance from radar of the peak of IWC_g.

Date	IOP	TA	2-DVD/S	2-DVD/C	Strokes	ML [m]	Mode [km]
3 Sep 2012			NA	NA	195(5166)	3568	84–96
4 Sep 2012			NA	NA	1202(3814)	3328	84–96
5 Sep 2012			NA	NA	941 (2181)	3466	84–96
13 Sep 2012	2	NEI-LT	342	38	3621(6594)	3716	72–84
9 Oct 2012			15	0	220(273)	3713	48–60
11 Oct 2012	12A	LT-CI	0	0	28(32)	3446	72–84
12 Oct 2012	12A	LT-CI	180	71	7011(8909)	3402	84–96
14 Oct 2012			0	0	4 (122)	3060	84–96
15 Oct 2012	13 (F20)	LT-CI-NEI	157	31	3388(6765)	2985	36–48
26 Oct 2012	16A & C(F20)	LT-CI-NEI	222	23	761 (1434)	3150	96–108
27 Oct 2012	16A & C	LT-CI-NEI	82	2	14 (5078)	3957	96–108

AMTD
8, 9241–9287, 2015

Table 4. Coefficients for the linear regression ($y = ax + b$) and coefficent of determination (R^2) obtained for the three case studies shown in Fig. 9. The first three parameters concerning the TAG obtaned from new scheme of HCA, while the second three parameters from TAG obtaned by the former HCA.

Date	a	b	R^2	a	b	R^2
13 Sep 2012	1.63×10^6	2.86×10^6	0.506	1.75×10^6	3.71×10^6	0.478
12 Oct 2012	1.23×10^6	1.03×10^7	0.824	1.82×10^6	2.68×10^7	0.807
15 Oct 2012	5.77×10^6	2.71×10^7	0.856	6.31×10^6	3.66×10^7	0.850

AMTD
8, 9241–9287, 2015

Table 5. The occurrence (from 16:00 to 20:25 UTC of 15 October) of the different kind of strokes detected by the LINET network is shown in the second column, while in the last column the R^2 of the linear correlation betweeen strokes and the total amount of IWC of graupel is listed.

Strokes	Occurrence	R^2
−CG	1834	0.73
+CG	732	0.66
IC	518	0.48
Total	3084	0.86

AMTD
8, 9241–9287, 2015

Table 6. Contingency tables between the presence of strokes (St) occurred over Sapienza site (within 10 km of ray in 1 min) and convective or stratiform (CS) minutes recorded by 2-DVD (a), while strokes and presence of IWC_g greater than 0 g cm^{-3} estimated by Polar 55C over the Sapienza site (Gr) is shown in (b).

convective or stratiform minutes recorded by 2-DVD (a)			IWC_g greater than 0 g cm^{-3} (b)		
	Yes(St)	No(St)		Yes(St)	No(St)
conv.	20	11	Yes(Gr)	58	12
strat.	21	134	No (Gr)	6	5

AMTD
8, 9241–9287, 2015

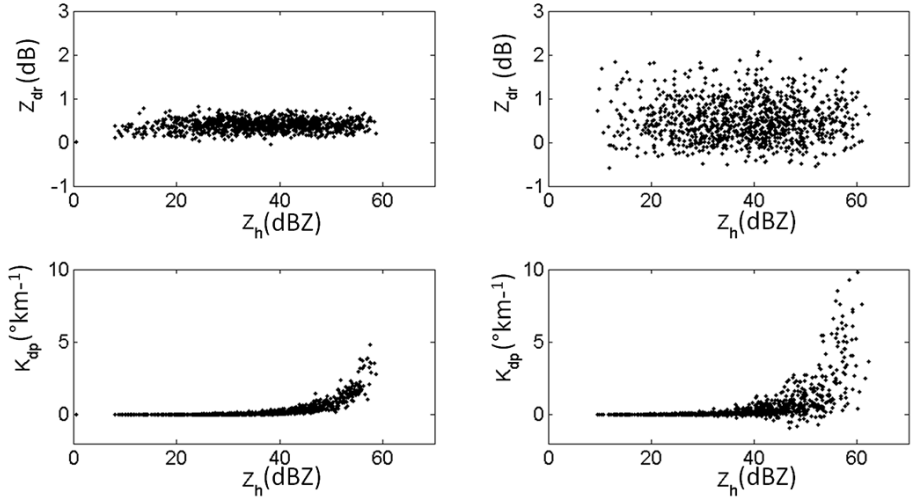

Figure 1. Scatter plots of C-band differential reflectivity (top) and specific differential phase shift (bottom) vs. reflecticity factor obtained by T-matrix simulations for graupel. Left panels are referred to spheroid graupel simulations (details in second column of Table 1), while right panels are referred to conical graupel simulations (third column of Table 1).

AMTD
8, 9241–9287, 2015

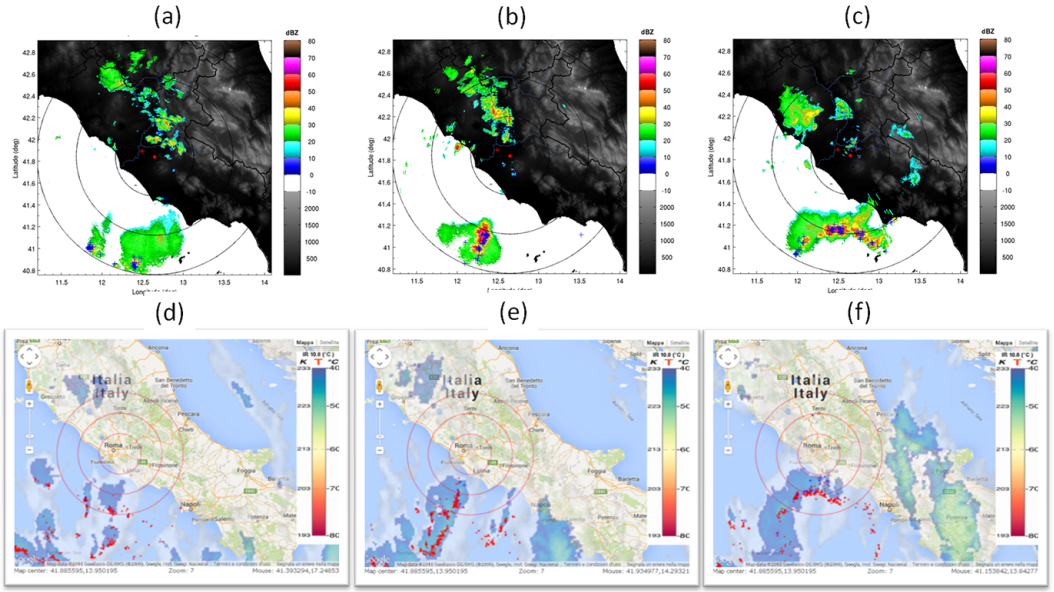

Figure 2. Polar 55C Z_h (1.6° of elevation angle) at 20:00 UTC **(a)**, 21:00 UTC **(b)** and 22:30 UTC **(c)** concerning the 13 September 2012. Superimposed are the strokes occurred in 5 min (blue cross). In **(d–f)** panels are shown the respectively infrared (IR) MSG images at 10.8 µm on google maps using MAMS tool (Petracca et al., 2013). Superimposed are the LINET strokes (CG in red circle; IC in blue circle) occurred in 15 min and Polar 55C range rings respectively at (40, 80 and 120 km).

AMTD
8, 9241–9287, 2015

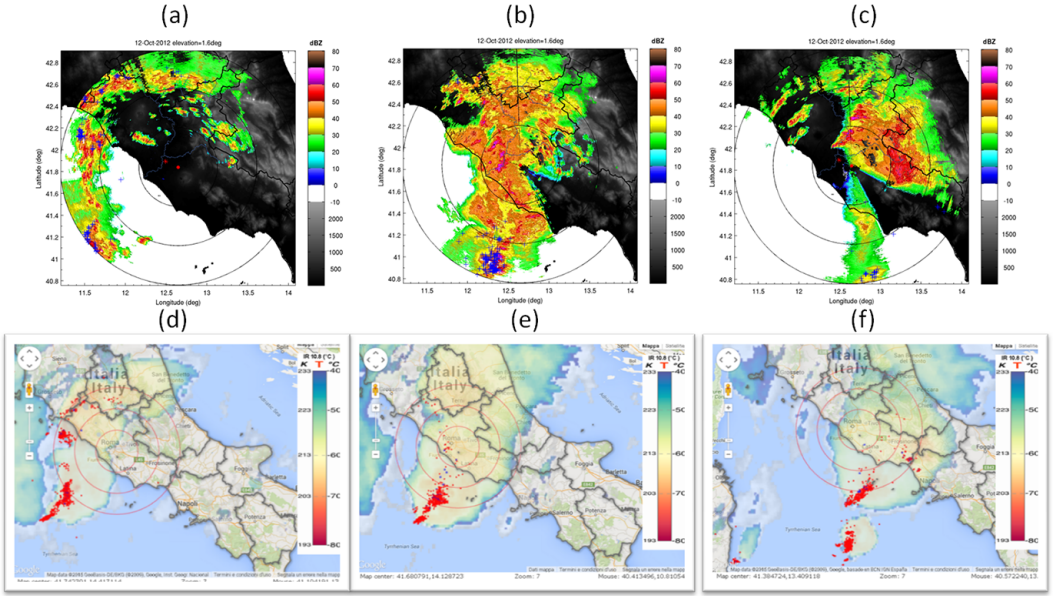

Figure 3. As in Fig. 2 for the 12 October 2012 at 03:00 UTC **(a)** and **(d)**, 04:30 UTC **(b)** and **(e)** and 06:00 UTC **(c)** and **(f)**.

AMTD
8, 9241–9287, 2015

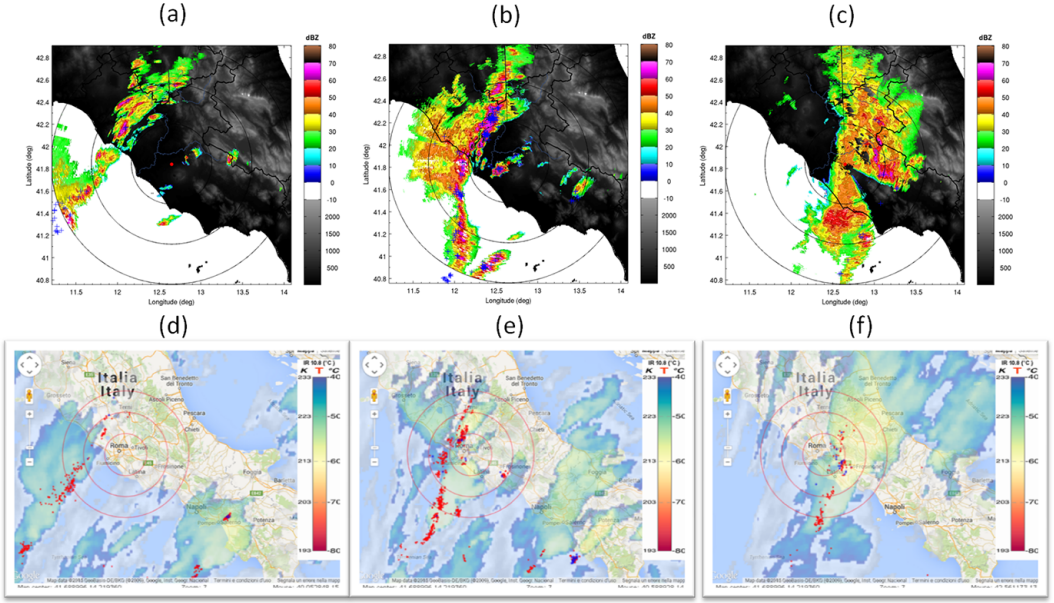

Figure 4. As in Fig. 2 for the 15 October 2012 at 16:00 UTC **(a)** and **(d)**, 17:30 UTC **(b)** and **(e)** and 19:10 UTC **(c)** and **(f)**.

AMTD
8, 9241–9287, 2015

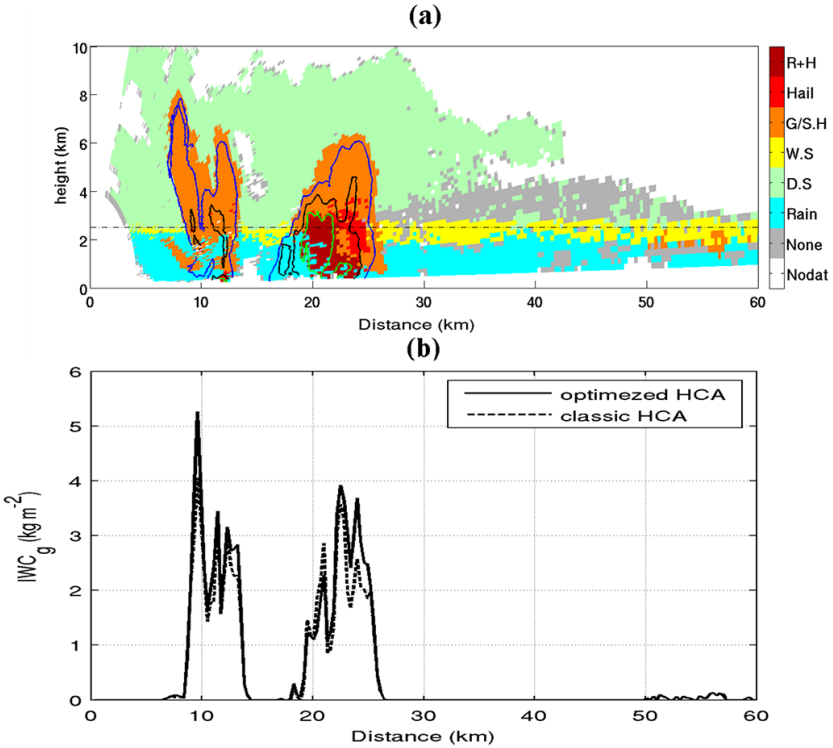

Figure 5. Polar 55C RHI scanning collected at 17:55 UTC of 15 October 2012 for the azimuth at 293° along the Sapienza site resampled radar measurements at a 300 m range resolution. Fuzzy logic HCA optimized for graupel **(a)**, with the color bar as follows: white is no data, gray is no classified, light blue is rain, green is dry snow, yellow is wet snow, orange is graupel and small hail, red is hail and dark red is hail rain mix. Superimposed are the Z_h contour at 40 dBZ (blue line), 50 dBZ (black solid line), 55 dBZ (green solid line). The black dash-dot line is the 0 deg level. **(b)** Columnar IWC of graupel refferred to RHI obtained by optimezed the new scheme of graupel detection (black solid line) and to the classical HCA (black dashed line) is plotted.

AMTD
8, 9241–9287, 2015

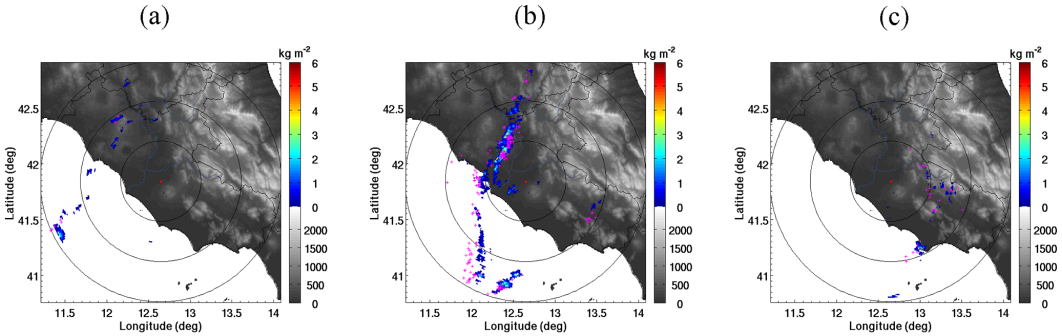

Figure 6. The columnar graupel IWC estimated from Polar 55C at 16:00 UTC **(a)**, 17:30 UTC **(b)** and 19:20 UTC **(c)** of the 15 October 2012. Strokes detected by LINET network are represented by the magenta crosses.

AMTD
8, 9241–9287, 2015

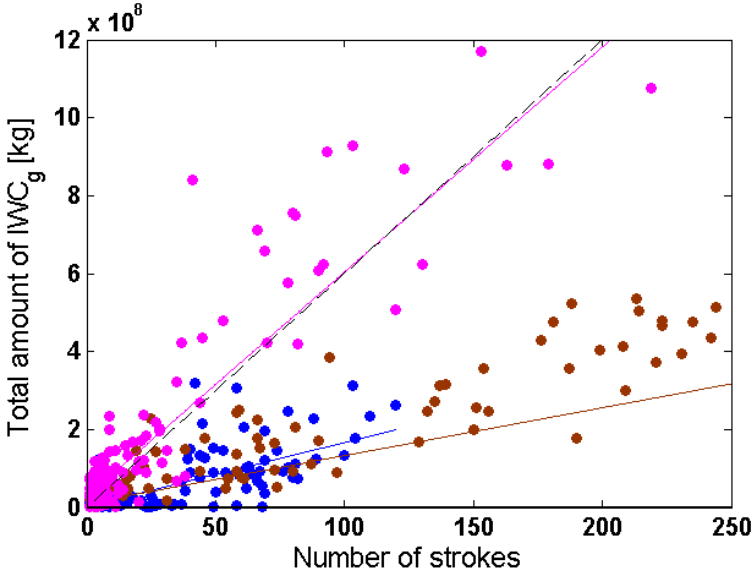

Figure 7. The total number of strokes detected by LINET in the area coverage by Polar 55C in relation to the total amount of graupel IWC above the ML detected by radar between for 13 September 2012 (blue), 12 October 2012 (brown) and 15 October 2012 (magenta). Points related to each days are fitted with linear regression (solid line). Black dashed line is the threshold converted in TAG found by Formenton et al. (2014).

AMTD
8, 9241–9287, 2015

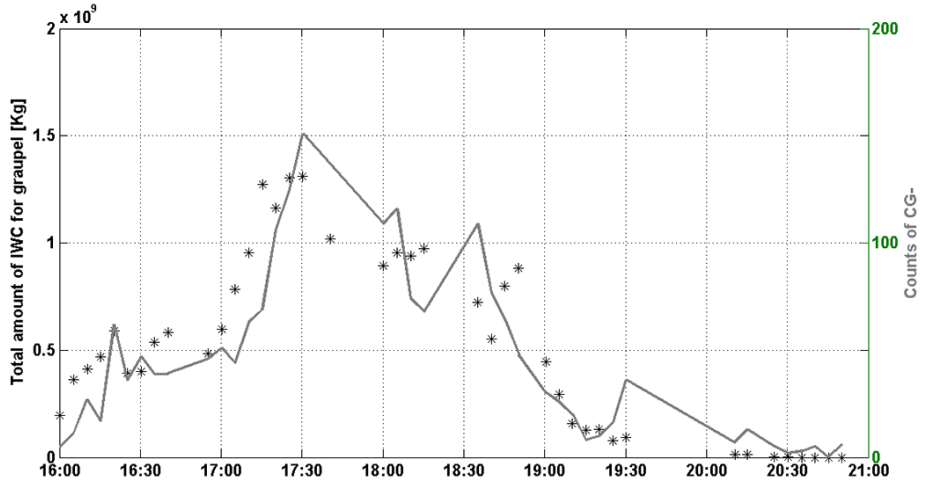

Figure 8. The time evolution of the total amount of IWC above 0° isothermal (black stars and *y* axis on the left side) and the counts of −CG (gray line and *y* axis on the right side) occurred on 15 October 2012 within the Polar 55C area coverage.

AMTD
8, 9241–9287, 2015

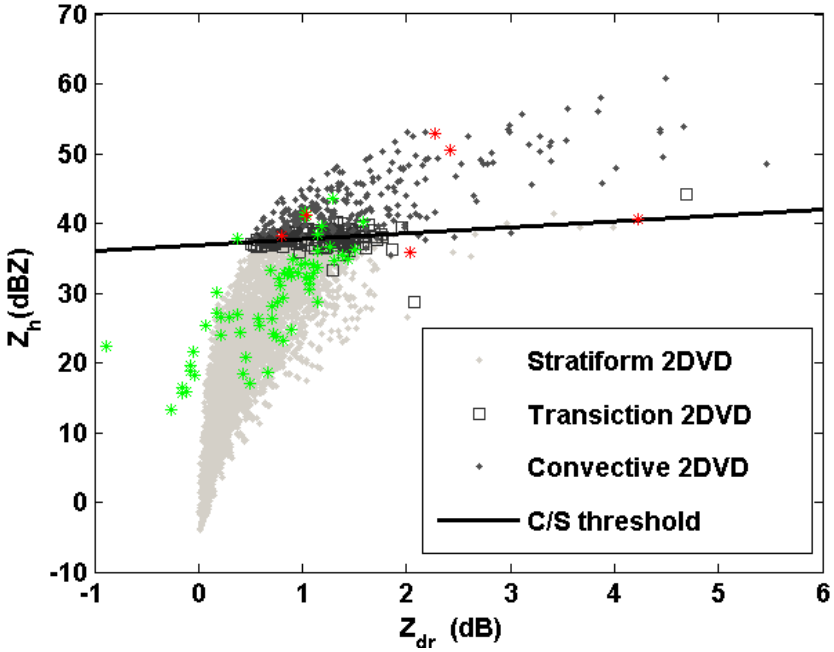

Figure 9. Plot of the Z_h, and Z_{dr} obtained from the disdrometer measured RSD through e.m. simulation for all the datasets collected by 2-DVD (grey markers). The different gray shades are based on the C/S classification of Bringi et al. (2009). The C/S threshold is $Z_h = 36.86 + 0.84Z_{dr}$. The rainy minutes above the C/S threshold are classified as convective, and the ones below as stratiform. Colored markers are the Polar 55C measurements collected over Sapienza site (elevation 1.6 deg) for all the database classified according Baldini and Gorgucci (2006).

AMTD
8, 9241–9287, 2015

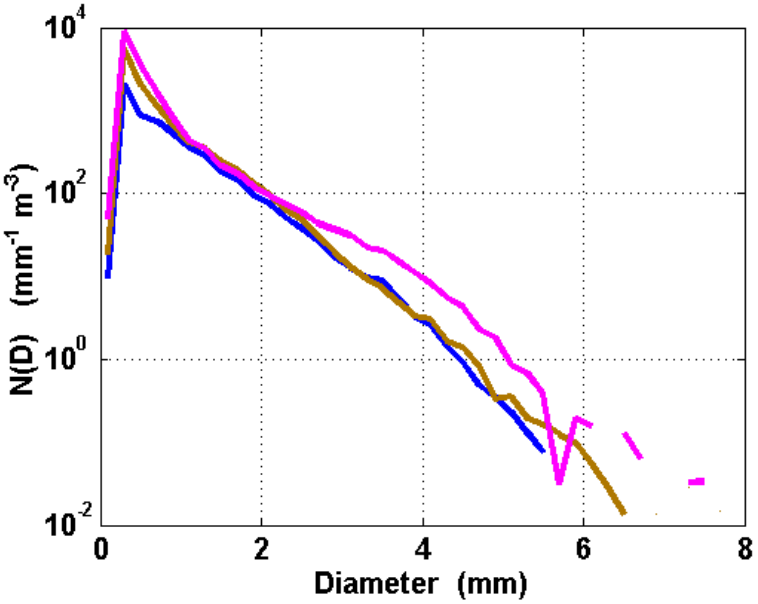

Figure 10. Each colored solid line represents the RSD averaged over the convective minutes of 13 September 2012 (blue), 13 October 2012 (brown) and 15 October 2012 (magenta).

AMTD
8, 9241–9287, 2015

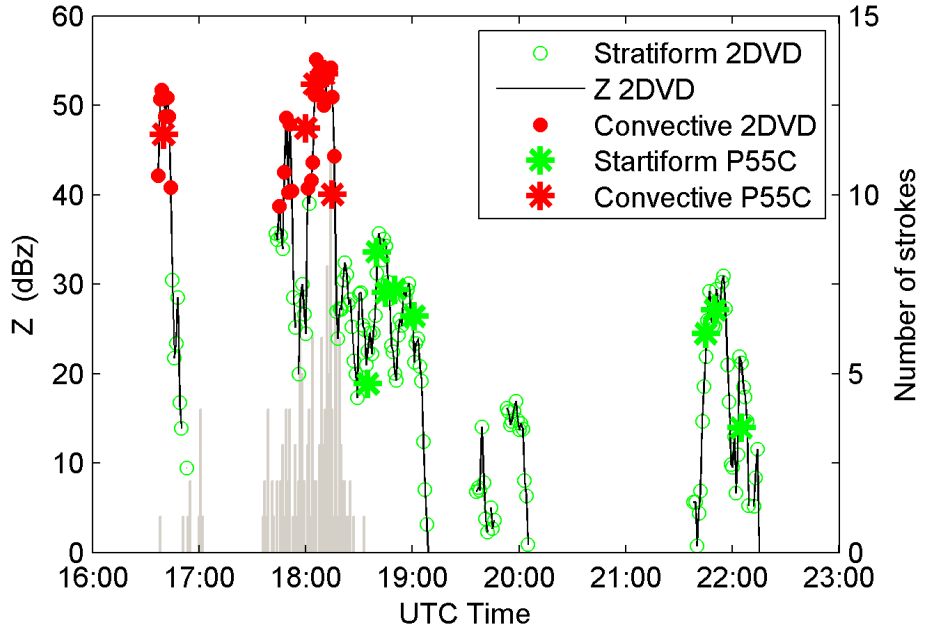

Figure 11. Time series of the reflectivity factors and the number of LINET strokes. Circles represent reflectivity factor computed from the RSD measured by the 2-DVD, while stars represent the values measured by the Polar 55C radar over Sapienza site. Green markers indicate stratiform rain, while the red markers indicate convective rain classified with the S/C trhreshold. Finally, the grey bars are the number of strokes registered in 1 min in a circular area of 10 km radius centered at the Sapienza site (2-DVD position).

AMTD
8, 9241–9287, 2015